



## A rational approach to elucidate human monoamine oxidase molecular selectivity



Giuseppe Felice Mangiatordi <sup>a</sup>, Domenico Alberga <sup>b</sup>, Leonardo Pisani <sup>a</sup>, Domenico Gadaleta <sup>a</sup>, Daniela Trisciuzzi <sup>a</sup>, Roberta Farina <sup>a</sup>, Andrea Carotti <sup>c</sup>, Gianluca Lattanzi <sup>d,e</sup>, Marco Catto <sup>a</sup>, Orazio Nicolotti <sup>a,\*</sup>

<sup>a</sup> Dipartimento di Farmacia-Scienze del Farmaco, Università di Bari 'Aldo Moro', Via Orabona, 4, 70126 Bari, Italy

<sup>b</sup> Institut de Recherche de Chimie Paris CNRS Chimie ParisTech, PSL Research University, 11 rue P. et M. Curie, F-75005 Paris 05, France

<sup>c</sup> Dipartimento di Scienze Farmaceutiche, Università degli Studi di Perugia, Piazza Università 1, Perugia 06123, Italy

<sup>d</sup> Physics Department, University of Trento, via Sommarive 14 Povo, Trento 38123, Italy

<sup>e</sup> Trento Institute for Fundamental Physics and Applications (INFN-TIFPA), via Sommarive 14 Povo, Trento 38123, Italy

### ARTICLE INFO

#### Article history:

Received 9 November 2016

Received in revised form 27 January 2017

Accepted 5 February 2017

Available online 07 February 2017

#### Keywords:

Drug design

Molecular selectivity

Molecular dynamics

MM-GBSA

Coumarin derivatives

MAO

### ABSTRACT

Designing highly selective human monoamine oxidase (hMAO) inhibitors is a challenging goal on the road to a more effective treatment of depression and anxiety (inhibition of hMAO-A isoform) as well as neurodegenerative diseases (inhibition of hMAO-B isoform). To uncover the molecular rationale of hMAOs selectivity, two recently prepared 2*H*-chromene-2-ones, namely compounds **1** and **2**, were herein chosen as molecular probes being highly selective toward hMAO-A and hMAO-B, respectively. We performed molecular dynamics (MD) studies on four different complexes, cross-simulating one at a time the two hMAO-isoforms (dimer embedded in a lipid bilayer) with the two considered probes. Our comparative analysis on the obtained 100 ns trajectories discloses a stable H-bond interaction between **1** and Gln215 as crucial for ligand selectivity toward hMAO-A whereas a water-mediated interaction might explain the observed hMAO-B selectivity of compound **2**. Such hypotheses are further supported by binding free energy calculations carried out applying the molecular mechanics generalized Born surface area (MM-GBSA) method and allowing us to evaluate the contribution of each residue to the observed isoform selectivity. Taken as whole, this study represents the first attempt to explain at molecular level hMAO isoform selectivity and a valuable yardstick for better addressing the design of new and highly selective MAO inhibitors.

© 2017 Elsevier B.V. All rights reserved.

### 1. Introduction

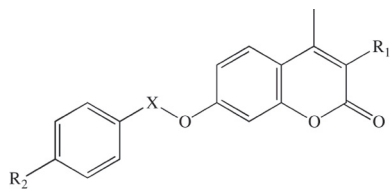
Monoamine oxidases (MAOs) are flavoproteins regulating the level of biogenic amines (e.g. dopamine (DA), noradrenalin (NA), adrenaline (AD), 2-phenylethylamine (PEA) and serotonin (5-HT)) and dietary amines (e.g. tyramine) in mammals by catalyzing their oxidative deamination (Weyler et al., 1990 and Shih et al., 1999). Expressed in different peripheral tissues and in the brain, MAOs are outer mitochondrial membrane enzymes that exist in two known and fully characterized isoforms, namely MAO-A and MAO-B (Shih et al., 1999 and Westlund et al., 1985). 5-HT, neurotransmitter proved to be crucial in human depression, is primarily metabolized by MAO-A that prevails in catecholaminergic neurons, while MAO-B, predominating in serotonergic neurons, reduces the levels of PEA preferentially. Both the isoenzymes are able to catabolize DA, AD and NA at similar rates (Youdim et al., 2006). The MAO well-established reputation as therapeutic target (Youdim et al., 2006 and Kumar et al., 2016) is closely related to the

specific function of both isoforms: MAO-A selective inhibitors are clinically administered as anxiolytics and antidepressants (Casacchia et al., 1984; van Vliet et al., 1992 and Baldessarini, 1989) while MAO-B selective inhibition is typically used for the treatment of the Parkinson's disease (PD) early symptoms (Youdim and Bakhle, 2006). Furthermore, recent studies demonstrated the involvement of both MAO-A and MAO-B into the pathogenesis and progression of heart failure, being both isoforms responsible for an enhanced aldehyde metabolism, nor-epinephrine catabolism and ROS production (Kaludercic et al., 2010 and Kaludercic et al., 2013). A renewed interest toward MAOs is now growing in the field of anti-Alzheimer medicines, claiming for the putative efficacy of MAOs inhibition in reducing ROS toxicity and oxidative stress (Riederer et al., 2004; Pisani et al., 2011 and Farina et al., 2015). Unfortunately, the earliest MAO inhibitors showed low isoform selectivity, thus causing severe side effects associated to their activity in peripheral tissues such as liver, placenta, intestine and lung (Saura et al., 1996). In particular, hypertensive drug-induced crises have been ascribed to the increased effect of sympathomimetic amines such as tyramine (mainly present in red wine and cheese and hence triggering the so-called "cheese-effect") that is not scavenged by gastrointestinal MAO-

\* Corresponding author.

E-mail address: [orazio.nicolotti@uniba.it](mailto:orazio.nicolotti@uniba.it) (O. Nicolotti).

A when blocked by non-selective and irreversible MAO inhibitors (Anderson et al., 1993). Such important side effects can be strongly reduced by administrating reversible inhibitors with high MAO-isoform selectivity. This holds true both for antidepressants (MAO-A selective) and MAO inhibitors administrated to treat the early symptoms of PD (MAO-B selective). Indeed, a higher isoform selectivity of the inhibitor might consent the use of a lower therapeutic dose thus strongly diminishing possible adverse effects. Research efforts over last years allowed designing potent and more selective MAO-A and MAO-B inhibitors (Pisani et al., 2015, Carotti et al., 2002, Santana et al., 2006, Hassan et al., 2006, La Regina et al., 2007, Binda et al., 2007, Gökhan-Kelekçi et al., 2009, Matos et al., 2009, Matos et al., 2010, Karuppasamy et al., 2010, Pisani et al., 2016a and Wang et al., 2015). Nevertheless, a suitable model allowing to rationally approach the selectivity issue is still missing, although the structural information of both human isoforms in complex with inhibitors, which are available in the Protein Data Bank (PDB), unveiled some relevant dissimilarities between the two isoforms. In particular, besides differing in terms of primary sequence (72% sequence identity) (Bach et al., 1988), tissue distribution, and sensitivity to substrates and inhibitors, MAO-A and MAO-B show remarkable differences in the shape of their active sites (Kalgutkar et al., 2001). Unlike MAO-A showing a monopartite cavity (De Colibus et al., 2005 and Son et al., 2008), MAO-B has a bipartite active site so that the substrate/ligand has to negotiate a small entrance room before entering the second and larger inner cavity where FAD is accommodated (Hubálek et al., 2005). Two “gate-keeper” residues, namely Ile199 and Tyr326, are responsible for such bipartite shape that can be lost upon binding of specific ligands able to induce conformational changes altering the cavity structure (Hubálek et al., 2005). In MAO-A, Ile199 and Tyr326 are replaced by Phe208 and Ile335, respectively (the numbering is referred to human isoforms) and the substrate/ligand is thus not forced to cross a small entrance room to bind to the enzyme. MAO-A cavity is, in fact, characterized by a unique and wider hydrophobic pocket containing FAD (De Colibus et al., 2005 and Son et al., 2008). Taking advantage of such structural differences and aimed at designing isoform-selective inhibitors, our research group has put great efforts in the last years on the synthesis of several MAO inhibitors with the aim to elucidate the mechanistic rationale behind MAO-A and MAO-B selective block. In particular, 2*H*-chromene-2-one derivatives, better known as coumarins, have been thoroughly studied as selective and potent MAO-A (Pisani et al., 2013a) and MAO-B (Catto et al., 2006; Pisani et al., 2009; Pisani et al., 2013b and Pisani et al., 2016b) inhibitors. More specifically, the presence of a planar backbone allows an efficient lodgement into both MAO-A and MAO-B catalytic sites. Furthermore, 2*H*-chromen-2-one is a versatile heterocycle which can be easily functionalized with a high degree of chemical diversity. However, the molecular mechanisms underlying the observed isoform selectivity have not been fully elucidated yet. This was likely due to fact that our design was mostly assisted by molecular docking, a simulating technique very effective in providing reliable binding poses but in this case inadequate for deriving a trustable selectivity model. Such failure can be likely ascribed to the main limit of this computational technique: it totally (or almost) assumes a rigid protein structure. Nevertheless, it is acknowledged that a protein can experience specific conformational rearrangements upon ligand binding so that its dynamic behavior should be taken into account in order to have a realistic picture of the ligand binding mode (Nicolotti et al., 2009 and Nicolotti et al., 2008). To properly approach this point, in this work we carried out extensive MD simulations, nowadays considered the method of choice for investigating the dynamics of biomolecules (Karplus and McCammon, 2002 and Alberga and Mangiatordi, 2016). Two 2*H*-chromene-2-ones derivatives designed and prepared by our group (**1** and **2**, highly selective compounds toward MAO-A and MAO-B, Table 1) were employed as molecular probes for investigating the molecular mechanisms underpinning their binding specificity. Notice that biological assays were performed following an already published protocol (Pisani et al., 2016a). The comparative analysis of the

**Table 1**Structures and inhibitory activity on hMAO-A and hMAO-B of compounds **1** and **2**.


Ligand	R <sub>1</sub>	R <sub>2</sub>	X	hMAO-A <sup>a</sup>	hMAO-B <sup>a</sup>
<b>1</b>	H	NO <sub>2</sub>	SO <sub>2</sub>	3.4	2692
<b>2</b>	Cl	H	CH <sub>2</sub>	135	0.85

<sup>a</sup> Expressed as IC<sub>50</sub> (nM).

100 ns MD trajectories obtained from the resulting systems allowed us to get important insights into the specificity of the protein-ligand interactions in MAO-A and MAO-B. To the best of our knowledge, this study represents the first attempt to challenge the MAO isoform-selectivity by comparative MD simulations, a strategy already proved to be able to understand and interpret ligand selectivity toward other targets (Wang et al., 2005; Zeng et al., 2008; Martínez et al., 2009 and Hu and Wang, 2014). Moreover, for the first time, MD simulations have been carried out on the dimeric structures of the two MAO isoforms, embedded in the lipid bilayer, the natural environment of the two enzymes likely influencing the observed conformational changes. The results are discussed in the perspective of designing new and more isoform selective inhibitors.

## 2. Methods

### 2.1. Docking Simulations

Crystal structures of hMAO-A with Harmine (PDB code: 2Z5X (Son et al., 2008)) and hMAO-B with Isatin (PDB code: 1OJA (Binda et al., 2003)) were retrieved from the Protein Data Bank (PDB) as targets for preliminary docking studies. Protein structures were prepared using the Protein Preparation Wizard (Sastry et al., 2013) available from Schrödinger Suite v2015-4 (Schrödinger Release 2015-4, 2015) and allowing us: 1) to remove the co-crystallized ligands, 2) to add missing hydrogen atoms and 3) to determine the optimal protonation states for histidine residues at physiological pH. The obtained files were used for docking simulations performed by GOLD v5.2 (Jones et al., 1997) on compounds **1** and **2** on both crystal structures. Following protocols validated in our previous papers (Catto et al., 2006 and Pisani et al., 2009), GoldScore was selected as fitness function and eight water molecules were explicitly considered during the docking runs within the hMAO-B binding site. Furthermore, a spherical grid having a radius of 12 Å originating from the center of mass of the cognate ligands was used.

### 2.2. From X-ray Structures to Model Systems Preparation

The same crystal structures selected for docking simulations (2Z5X (Son et al., 2008) and 1OJA (Binda et al., 2003)) were chosen as starting point for building the model systems subjected to MD simulations. Notice that the crystal structure of hMAO-A contains only one monomer so that the dimeric structure for this isoform was obtained using the hMAO-B dimer as template for chains positioning. In addition, the full-length homodimer of hMAO-A contains 527 residues in each monomer while that of hMAO-B 520 residues. However, as far as hMAO-A crystal structure is concerned, the chain includes residues His12 to Leu524 while in the h-MAO-B crystal structure chain A includes residues Asn3 to Ile501 and chain B includes residues Asn3 to Ile496. Following the approach by Allen and Bevan (Allen and Bevan, 2011), missing C-terminal residues were added to the model systems and dihedral angles

characteristic of an  $\alpha$ -helix were imposed to correctly reflect the transmembrane nature of the residues. Indeed, both isoforms are anchored to the mitochondrial membrane by means of two C-terminal helical tails (one for each chain) so that the presence of such residues is essential for obtaining a realistic model. Each dimer was pretreated using the Protein Preparation module included in the Schrödinger Suite v2015-4 (Schrödinger Release 2015-4, 2015) to add missing hydrogen atoms and detect the correct protonation state of histidine residues. The membrane plug-in of VMD (Visual Molecular Dynamics) software (Humphrey et al., 1996) was used for building a  $110 \times 135 \text{ \AA}^2$  POPC (1-palmitoyl,2-oleoyl-sn-glycero-3-phosphocholine) bilayer patch, with the membrane normal along the z-axis. Subsequently, the dimers were manually embedded in the bilayer and lipid molecules within  $0.8 \text{ \AA}$  of heavy atoms of the protein were removed. Following a previously published protocol (Alberga et al., 2014 and Mangiatordi et al., 2015), the systems were incorporated into a periodic box of TIP3P water molecules (Jorgensen et al., 1983) extended by  $18 \text{ \AA}$  in each direction from all protein atoms using the “solvate” plugin of VMD and neutralized adding  $\text{Na}^+$  and  $\text{Cl}^-$  ions using the VMD’s “autoionize” plugin, generating a 150 mM ionic concentration. The investigated ligands were placed inside the binding pocket of the two proteins using the poses obtained from docking simulations. The final obtained systems contains 182,686 atoms for hMAO-A and 191,957 atoms for hMAO-B (number computed considering as ligand compound **1**). These systems were again equilibrated with protein atoms and crystallographic water molecules at fixed positions for another 200 ps. The obtained system was finally relaxed for 200 ps, applying harmonic restraints only to the protein atoms (force constant of  $1 \text{ kcal/mol \AA}^{-2}$ ).

### 2.3. Molecular Dynamics Simulations

All MD simulations were performed using NAMD 2.10 (Phillips et al., 2005) and the CHARMM36 force field (Huang and MacKerell, 2013). An exception is represented by the FAD cofactor and the two ligands, all parameterized using the CHARMM generalized Force-Field (CGenFF) (Vanommeslaeghe et al., 2010 and Yu et al., 2012) and the Restrainted electrostatic potential (RESP) model (Bayly et al., 1993) for charges, obtained at the HF/6-31G(d,p) level of theory and using the Gaussian09 package (Gaussian 09, 2009). The SHAKE algorithm was employed to constrain all R-H bonds. Periodic boundary conditions were applied in all directions. A non-bonded cut-off of  $12 \text{ \AA}$  was used, whereas the Particle-Mesh-Ewald (PME) (Darden et al., 1993) was employed to include the contributions of long-range interactions. All simulations were performed in an isothermal-isobaric ensemble (1 atm, 310 K) with a Nosè-Hoover Langevin barostat (Feller et al., 1995) (oscillation period 200 fs, decay coefficient 100 fs) and a Langevin thermostat (Adelman and Doll, 1976) (damping coefficient  $1 \text{ ps}^{-1}$ ). The time step was set to 2 fs, and coordinates were saved every 1000 steps (2 ps). For all the considered systems, the equilibration of the structure required less than 5 ns and, thus, the first 5 ns were removed from the analysis of the obtained 105 ns of trajectory. Root Mean Square Deviations (RMSDs) and Root Mean Square Fluctuations (RMSFs) were obtained after alignment of the trajectory to all the C-alpha atoms belonging to the monomer under investigation. All simulations were performed on the FERMI supercomputer at CINECA, Italy.

### 2.4. Binding Free Energy Calculations

The binding free energies ( $\Delta G$ ) between protein and ligands were computed by applying the MM-GBSA methodology (Kollman et al., 2000; Genheden and Ryde, 2015 and Hou et al., 2011) to the MD trajectories, as implemented in AmberTools15 (Case et al., 2015). In particular, for each considered complex, 1000 snapshots were chosen from the trajectory (interval of 100 ps). Each snapshot was then subjected to the following procedure: i) stripping of all water molecules and

ii) computation of the free energy of each species (complex, receptor and ligand), iii) computation of the binding free energy as:

$$\Delta G = G_{\text{complex}} - (G_{\text{protein}} + G_{\text{ligand}}) \quad (1)$$

where  $G_{\text{complex}}$ ,  $G_{\text{protein}}$  and  $G_{\text{ligand}}$  are the free energies of complex, protein and ligand respectively. In particular  $\Delta G$  was computed as the sum of three contributes:

$$\Delta G = \Delta G_{\text{MM}} + \Delta G_{\text{solv}} - T\Delta S \quad (2)$$

where  $\Delta G_{\text{MM}}$  is the change in the molecular mechanics (MM) gas-phase binding energy,  $\Delta G_{\text{solv}}$  is the solvation free energy and  $-T\Delta S$  is the conformational entropic contribution. Moreover both  $\Delta G_{\text{MM}}$  and  $\Delta G_{\text{solv}}$  are further divided into two parts:

$$\Delta G_{\text{MM}} = \Delta G_{\text{vdw}} + \Delta G_{\text{ele}} \quad (3)$$

where  $\Delta G_{\text{vdw}}$  and  $\Delta G_{\text{ele}}$  are the van der Waals and the electrostatic energies respectively.

$$\Delta G_{\text{solv}} = \Delta G_{\text{pol}} + \Delta G_{\text{nonpol}} \quad (4)$$

where  $\Delta G_{\text{pol}}$  and  $\Delta G_{\text{nonpol}}$  are the polar and nonpolar component of the solvation free energy.

$\Delta G_{\text{pol}}$  was calculated using the GB model implemented in AmberTools15. The dielectric constants of the solute and of the solvent were set to 1.0 and 80.0 respectively.  $\Delta G_{\text{nonpol}}$  was computed as

$$\Delta G_{\text{nonpol}} = \gamma \text{SASA} + \beta \quad (5)$$

where SASA is the solvent-accessible surface area with a probe radius of  $1.4 \text{ \AA}$ .  $\gamma$  and  $\beta$  are empirical constants set to  $0.0072 \text{ kcal/mol \AA}^{-2}$  and  $0 \text{ kcal/mol}$  respectively.

Furthermore we calculated the free energy contributions of the enzyme residues to the binding free energy of the ligands. In this case the binding interaction of each ligand-residue pair can be represented as:

$$\Delta G_{\text{ligand-residue}} = \Delta G_{\text{vdw}} + \Delta G_{\text{ele}} + \Delta G_{\text{pol}} + \Delta G_{\text{nonpol}} \quad (6)$$

where the polar solvation contribution ( $\Delta G_{\text{pol}}$ ) where calculated using the GB parameters developed by Onufriev et al. (Onufriev et al., 2000).

## 3. Results and Discussion

### 3.1. Preliminary Docking Studies

MD simulations were carried out considering as molecular probes two reversible inhibitors showing high isoform selectivity on human MAO-A (hMAO-A) and human MAO-B (hMAO-B), namely compounds **1** and **2**. As shown in Table 1, the two ligands share a coumarin moiety linked to an aromatic substituent by means of two different linkers at position 7, namely a sulfonate ester in **1** and an oxy-methylene in **2**.

As a first step of the work, **1** and **2** were subjected to docking simulations aimed at finding a reliable starting conformation in hMAO-A and hMAO-B binding sites for the following MD simulations. Fig. S1 (see the Supporting Information) shows the top-scoring poses obtained for both ligands in hMAO-A and hMAO-B crystal structures, PDB codes 2Z5X (Son et al., 2008) and 1OJA (Binda et al., 2003) respectively (see the experimental section for methodological details). The posing of both ligands depends on the considered MAO isoform. More specifically, the presence of Phe208 and Ile335 as gate-keepers in MAO-A forces the ligand in an “arched” conformation (Fig. S1A–C) while a more extended pose can be detected in MAO-B (Fig. S1B–D).

### 3.2. Molecular Dynamics Simulations

Starting from the obtained docking poses, four different simulation systems were built and investigated:

1. Dimer of hMAO-A complexed with **1** (**hMAO-A vs 1**);
2. Dimer of hMAO-A complexed with **2** (**hMAO-A vs 2**);
3. Dimer of hMAO-B complexed with **1** (**hMAO-B vs 1**);
4. Dimer of hMAO-B complexed with **2** (**hMAO-B vs 2**).

#### 3.2.1. MD Simulations of **1** in hMAO-A and hMAO-B

With the aim to get insights into the conformational stability of **1** during the simulation, we monitored, as a first step of analysis of the obtained trajectories, the time-dependence of the Root Mean Square Deviations (RMSD) of such compound in h-MAO-A and h-MAO-B (Fig. 1A and B).

As clearly shown in Fig. 1A, in h-MAO-A, **1** experiences only slight fluctuations during the simulation (RMSF equal to 1.283 Å and 1.525 Å in monomers I and II, respectively). This observation suggests that, during the equilibration run, the ligand reaches a highly stable conformation. However, a more in-depth inspection of the obtained trajectory reveals that such conformations of equilibrium differ between the monomers, due to diverse conformational rearrangements occurring at the equilibration stage. As far as the monomer I is concerned, the conformational arrangement of the ligand allows to establish an H-bond interaction with the side chain of Gln215. Notably, this interaction was not seen in the obtained top-scoring docking pose as evident in Fig. 2A (distance between the H-bond acceptor and H-bond donor atoms equal to 5.2 Å).

Furthermore, the occurring conformational rearrangement does not involve the gate-keepers residues, whose conformations remain almost unchanged with respect to the one in the crystal structure (see Fig. 2A). More specifically, together with a reorientation of the  $-SO_2-$  group, during the equilibration run, a slight shift of the ligand takes place downwards closer to the FAD co-factor. In other words, the presence of a

sulfonate ester group, namely a linker with two strong H-bond acceptor oxygen atoms, implicates the loss of the “arched” conformation, typical of the coumarin-based MAO-A inhibitors. This is the result of a gain in terms of binding energy due to the H-bond interaction with Gln215, as unveiled by the binding energy calculations (see section 3.3). The stability and therefore the importance of this interaction are strongly supported by the time dependence of the distance between the H-bond donor (nitrogen atom of Gln215 side chain) and H-bond acceptor (oxygen atom of sulfonate ester group) during the entire simulation time. Importantly, distance values that are compatible with the H-bond interaction are noticeable along the entire trajectory and whenever the interaction is lost, it is re-established after a few picoseconds (see Fig. 2B). This strongly supports the robustness of the molecular hypothesis resulting from the detailed inspection of some selected frames: a conformational rearrangement of compound **1** allows the engagement of a strong and stable H-bond between its sulfonate ester group and the side chain of Gln215, an interaction non detectable based from previously performed docking simulations (Gökhan-Kelekçi et al., 2009; Catto et al., 2006; Chimenti et al., 2006 and Reis et al., 2016).

As above-mentioned, a different ligand conformation of equilibrium can be detected in monomer II during the simulation of hMAO-A vs **1**. A selected frame is shown in Fig. 2C: as in monomer I, an important conformational realignment occurs during the simulation. The ligand significantly changes its binding conformation with respect to the starting one and an important shift toward the FAD cofactor takes place. In this case, the new binding conformation allows establishing a water-mediated H-bond network involving the backbone of Ile180 and the side-chain of Tyr407. As evident comparing Fig. 2C and Fig. 2A, such conformation strongly differs from the one detected during the simulation of monomer I, being the sulfonate ester group of the ligand oriented in the opposite direction. Such difference in terms of binding mode is also confirmed by the absence of an H-bond interaction with Gln215 during the simulation. Importantly, the described water-mediated H-bond network is quite stable during the simulation: once the interaction is established, the involved water molecule remains

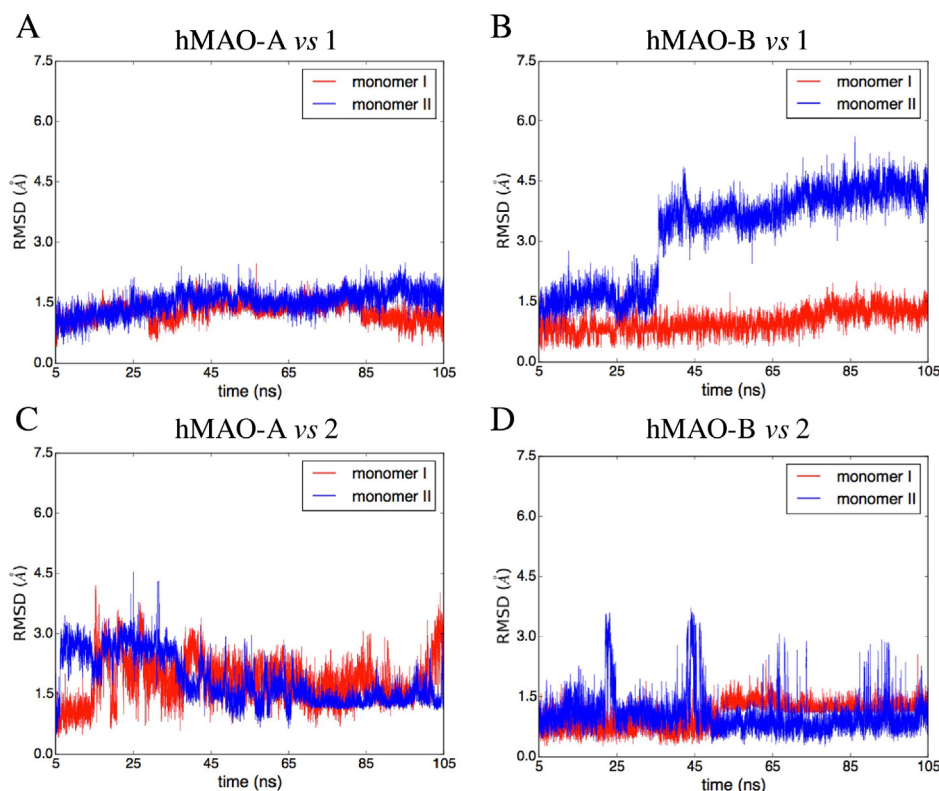
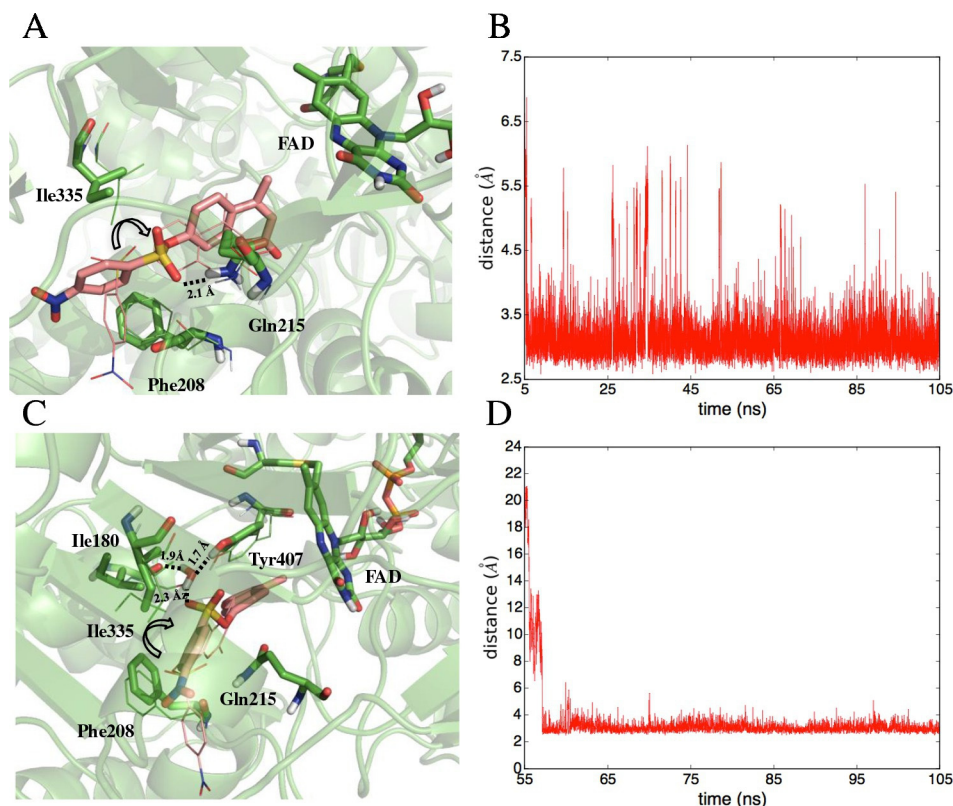


Fig. 1. Time-dependence of RMSD (Å) computed for compounds **1** and **2** in hMAO-A and hMAO-B. A) hMAO-A vs 1; B) hMAO-B vs 1; C) hMAO-A vs 2; D) hMAO-B vs 2.



**Fig. 2.** A) Selected frame showing the H-bond interaction involving the side chain of Gln215 and the sulfonate linker of compound **1** in hMAO-A (monomer I). B) Time-dependent evolution of the distance (Å) between the H-bond donor (nitrogen atom of Gln215 side chain) and H-bond acceptor (oxygen atom of the sulfonate linker of compound **1**) during the simulation of hMAO-A vs **1** (monomer I). C) Selected frame showing the H-bond interactions involving the side chain of Tyr407, the backbone of Ile180, a water molecule and the sulfonate linker of compound **1** in 1-hMAO-A (monomer II). D) Time-dependent evolution of the distance (Å) between the H-bond donor (oxygen atom of water) and H-bond acceptor (oxygen atom of the sulfonate linker of compound **1**) during the simulation (from 55 to 105 ns) of hMAO-A vs **1** (monomer II). For the sake of clarity, only polar hydrogen atoms are displayed. Compound **1**, FAD and important residues are rendered as sticks (selected frame) or lines (docking pose aligned to the selected frame). **1** is depicted with pink carbon atoms while important residues and FAD with green carbon atom. For each detected H-bond interaction (depicted by a dotted line) the distance between acceptor atom and hydrogen is reported. The arrow indicates the conformational rearrangement of **1** (starting from the top-scoring docking pose shown by thinner wire frames) that is required to engage the depicted H-bond interactions. (For interpretation of the references to colour in this figure legend, the reader is referred to the web version of this article.)

trapped within the binding site for the last 45 ns of simulation. This is evident in Fig. 2D showing the time-dependence of the distance between the H-bond acceptor atom (one oxygen atom of the sulfonate linker) and the H-bond donor atom (oxygen atom of the trapped water molecule) clearly indicating that the H-bond interaction is maintained until the end of the simulation.

In summary, the analysis of the trajectory resulting from MD simulations of hMAO-A vs **1** suggests the presence of two alternative binding modes for **1** in this isoform, the first involving a strong H-bond with Gln215, the second implicating a water-mediated interaction with Ile180 and Tyr407. Indeed, both these hypotheses are plausible and could justify, from a molecular point of view, the excellent activity toward hMAO-A ( $IC_{50}$  equal to 3.4 nM). In this respect, it is worth saying that two of the three involved residues (Gln215 and Tyr407) are also present in hMAO-B (Gln206 and Tyr398) and that the interaction with Ile180, replaced by Leu171 in hMAO-B, is played mostly by the backbone atoms. In order to gain molecular insights into the hMAO-A selectivity of **1**, the comparison with the trajectory resulting from MD simulations of hMAO-B vs **1** has been carried out. Again, as a first step, we computed the RMSD values of the ligand during the simulation of hMAO-B vs **1**. The obtained time-dependence suggests that the ligand is, consistently with the experimental data, less stable in hMAO-B (Fig. 1B) with respect to hMAO-A (Fig. 1A). This is especially evident in monomer II where, after about 35 ns, **1** assumes a new conformation of equilibrium with respect to the previous one resulting from the equilibration run. Such conformational rearrangement, involving again the shift of the ligand toward the FAD cofactor (see Fig. 3A),

takes place in monomer I during the equilibration run and the resulting conformational state is never lost during the entire simulation. In other words, **1**, differently from hMAO-A, assumes in hMAO-B a unique binding conformation in both the monomers, albeit belatedly in monomer II. A selected frame showing such binding conformation is shown in Fig. 3A: as in monomer II of hMAO-A, the conformational rearrangement allows establishing a water-mediated H-bond network involving the side chain of Tyr398 (Tyr407 in hMAO-A) and the backbone of Leu171 (Ile180 in hMAO-A). The stability of the detected water-mediated H-bond network is supported by the time-dependent evolution of the distance between the oxygen atom of the trapped water molecule and one oxygen atom of the sulfonate linker of compound **1** (see Fig. 3B). Importantly, no interaction can be found with Gln206 (Gln215 in hMAO-A) in both the monomers during the entire simulation thus suggesting that the interaction with such key residue could be responsible for the observed isoform selectivity. On the contrary, the same water-mediated H-bond network can be detected in both hMAO-A vs **1** and hMAO-B vs **1** thus putting forward this interaction as certainly relevant for the affinity of **1** but not determinant for the selectivity.

Building on these results, we can speculate that in hMAO-B the H-bond interaction with Gln206 is prevented because of the smaller size of its binding site (Youdim et al., 2006). At this regard, a crucial role seems to be played by a gate-keeper residue, namely Tyr326 that is replaced by Ile335 in hMAO A. The presence of such bulkier residue in hMAO-B prevents the rotation of the sulfonate linker, required to engage a H-bond interaction with Gln206 (see Fig. 4).

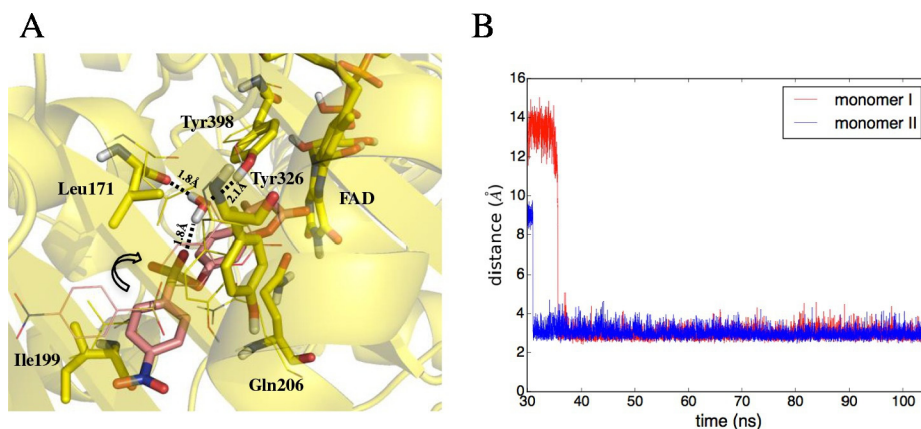


**Fig. 3.** A) Selected frame showing a water mediated interaction occurring in 1-hMAO-B between the sulfonate linker of the ligand and both the side chain of Tyr398 and the backbone of Leu171. B) Time-dependent evolution of the distance (Å) between the H-bond donor (oxygen atom of water) and H-bond acceptor (oxygen atom of the sulfonate linker of compound **1**) during the simulation of hMAO-B vs **1**. Compound **1**, FAD and important residues are rendered as sticks (selected frame) or lines (docking pose aligned to the selected frame). **1** is depicted with pink carbon atoms while important residues and FAD with yellow carbon atom. For each detected H-bond interaction (depicted by a dotted line) the distance between acceptor atom and hydrogen is reported. The arrow indicates the conformational rearrangement of **1** (starting from the top-scoring docking pose) that is required to engage the water-mediated interaction. (For interpretation of the references to colour in this figure legend, the reader is referred to the web version of this article.)

### 3.2.2. MD Simulations of **2** in hMAO-A and hMAO-B

The conformational stability of **2** in hMAO-A and hMAO-B was primarily assessed taking into account the time-dependence of their RMSD values during the performed simulations. As evident from Fig. 1, the ligand is characterized by a higher conformational stability in hMAO-B with respect to hMAO-A. This is also confirmed by the computed RMSF, being the values averaged along the two monomers equal to 1.828 and 1.063 Å, in hMAO-A and hMAO-B respectively. An in-depth analysis of the obtained trajectories clearly shows that **2** in monomer II of hMAO-B establishes a highly stable water-mediated interaction with FAD. Importantly, this interaction was not observed in hMAO-A vs **2**, thus giving a glimpse of a possible explanation of the selectivity of **2** toward hMAO-B. A selected frame extracted from the hMAO-B vs **2** trajectory (monomer II) is shown in Fig. 5A.

A conformational rearrangement occurring during the equilibration run allows establishing a water-mediated interaction with FAD. Such

conformational rearrangement mainly involves the ligand (moved forward with respect to the starting conformation, see Fig. 5A) whereas the gate-keepers residues remain almost frozen in the crystallographic conformation. In other words, the described water-mediated interaction results from the shifting of coumarin scaffold toward the FAD co-factor planar system. The stability of such interaction is supported by the time-dependent evolution of the distance between the H-bond acceptor atom of the ligand (carbonyl oxygen atom of the coumarin moiety) and the H-bond donor atom (oxygen atom of the trapped water molecule): from 50 ns to 105 ns of trajectory the interaction is almost kept and when lost (from 80 to 92 ns, see dashed lines in Fig. 5B) is quickly reestablished. It is worth noting that the same water-mediated interaction can be hypothesized after a visual inspection of a crystal structure of hMAO-B complexed with the cognate coumarin derivative (7-[(3-chlorobenzyl)oxy]-2-oxo-2H-chromene-4-carbaldehyde, PDB code 2V60), thus supporting the robustness of the hypothesis based

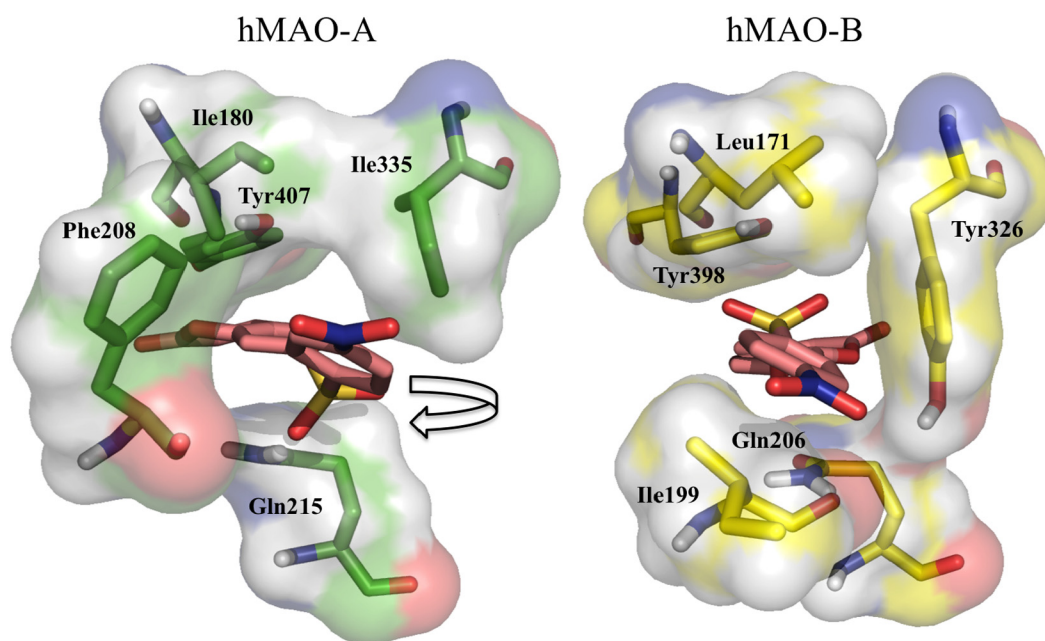


**Fig. 4.** Sketches of the binding sites in hMAO-A vs **1** and hMAO-B vs **1**. The arrow indicates the conformational rearrangement of **1** required to engage the depicted H-bond interaction with Gln215.

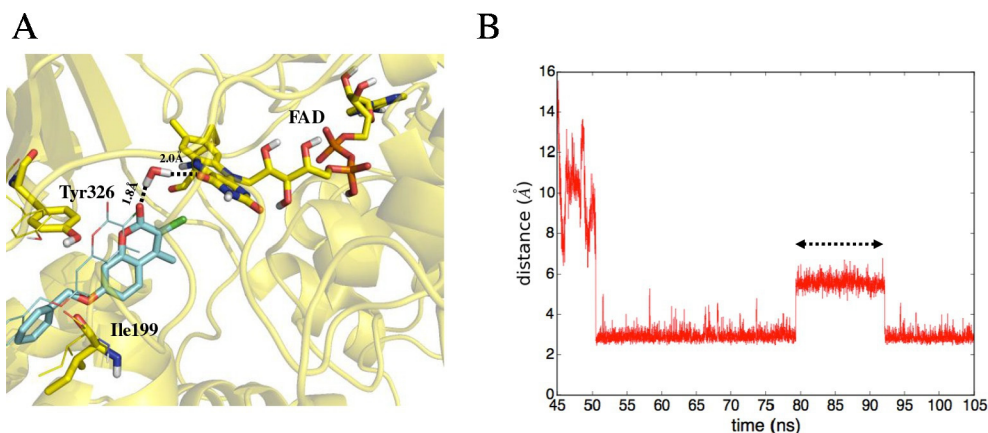


**Fig. 5.** A) Selected frame showing a water-mediated interaction occurring in hMAO-B vs **2** (monomer I) between the coumarin moiety of the ligand and the FAD cofactor. B) Time-dependent evolution of the distance (Å) between the H-bond donor (oxygen atom of water) and H-bond acceptor (carbonyl oxygen atom of the coumarin moiety of **2**) during the simulation of hMAO-B vs **2**. Compound **1**, FAD and important residues are rendered as sticks (selected frame) or lines (docking pose aligned to the selected frame). **2** is depicted with cyan carbon atoms while important residues and FAD with yellow carbon atoms. For each detected H-bond interaction (depicted by a dotted line) the distance between acceptor atom and hydrogen is reported. (For interpretation of the references to colour in this figure legend, the reader is referred to the web version of this article.)

on MD data. As far as the hMAO-A vs **2** MD system is concerned, the ligand is not able to establish the already described water-mediated interaction due to its arched conformation forcing the carbonyl oxygen atom of the coumarin moiety far away from the FAD cofactor (see Fig. S1C).

### 3.3. Binding Free Energy Analysis

To better elucidate the molecular mechanism driving the selective binding of the two examined ligands, we computed their binding affinity toward hMAO-A and hMAO-B by using the Molecular Mechanics/Generalized Born Surface Area (MM-GBSA) method (Kollman et al., 2000; Genheden and Ryde, 2015 and Hou et al., 2011). Notice that the computed binding free energies ( $\Delta G$ ) comprise different terms: i) van der Waals contribution to ligand binding ( $\Delta G_{vdw}$ ); ii) electrostatic contribution to ligand binding ( $\Delta G_{ele}$ ); iii) electrostatic contribution to the solvation free energy ( $\Delta G_{pol}$ ); iv) nonpolar contribution to the solvation free energy ( $\Delta G_{nonpol}$ ) and v) enthalpy variation upon ligand binding ( $\Delta H$ ). Tables 2 and 4 show the MM-GBSA results, which clearly indicate as the binding of **1** and **2** is thermodynamically allowed.

The dominant term driving the binding is  $\Delta G_{vdw}$ , which would suggest that in both the systems the affinity is mostly driven by the shape complementarity (hydrophobic interactions). This term rewards the drop in affinity due to the unfavorable electrostatic balance resulting from prevalence of the  $\Delta G_{pol}$  (unfavorable) compared to  $\Delta G_{ele}$  (favorable) term on the binding affinity. Consistently with its experimentally proved selectivity, **1** shows a larger binding free energy in hMAO-A ( $-22.07$  kcal/mol and  $-18.15$  kcal/mol in monomers I and II, respectively) with respect to hMAO-B ( $-16.45$  kcal/mol and  $-13.21$  kcal/mol in monomers I and II, respectively). Interestingly, the term  $\Delta G_{ele}$  shows the largest difference between the two isoforms,

**Table 2**  
Binding free energy contributions (kcal/mol) in hMAO-A vs **1** and hMAO-B vs **1**.

Terms	hMAO-A vs <b>1</b>		hMAO-B vs <b>1</b>	
	Monomer I	Monomer II	Monomer I	Monomer II
$\Delta G_{vdw}$	$-48.02(\pm 2.36)$	$-48.42(\pm 2.32)$	$-50.48(\pm 2.00)$	$-47.26(\pm 2.27)$
$\Delta G_{ele}$	$-18.95(\pm 4.42)$	$-16.10(\pm 3.60)$	$-10.23(\pm 2.32)$	$-11.69(\pm 3.00)$
$\Delta G_{pol}$	$32.39(\pm 2.84)$	$36.22(\pm 2.37)$	$32.86(\pm 2.20)$	$34.34(\pm 2.55)$
$\Delta G_{nonpol}$	$-6.80(\pm 0.17)$	$-6.82(\pm 0.15)$	$-6.76(\pm 0.12)$	$-6.53(\pm 0.23)$
$\Delta H$	$-41.38(\pm 3.12)$	$-35.13(\pm 2.94)$	$-34.61(\pm 2.36)$	$-31.15(\pm 2.85)$
$\Delta G$	$-22.07(\pm 3.12)$	$-18.15(\pm 2.94)$	$-16.45(\pm 2.36)$	$-13.21(\pm 2.85)$

being  $\approx -17$  kcal/mol in hMAO-A and  $\approx -11$  kcal/mol in hMAO-B irrespective of the considered monomer. Unlike affinity relying on hydrophobic interactions responsible for an unspecific binding, the selectivity is instead driven by the occurrence of properly oriented HB interactions (H-bond with Gln215 of MAO-A) that can more specifically drive the binding toward a given isoform. In this respect, a larger binding free energy is obtained for monomer I in both the enzymatic isoforms. As far as the hMAO-A vs **1** system is concerned, this evidence supports the hypothesis whereby, between the two observed binding conformations, that found in monomer I (showing a H-bond interaction with Gln215) can better explain the isoform selectivity of **1**. On this basis, we can reasonably assume that, between the two monomers, the one giving the largest binding free energy provides the most realistic picture of the binding mode. Building on this assumption, we performed a more detailed inspection of the energy contribution to the ligand binding due to each residue of monomer I belonging to the binding site. As shown in Table 3, the results confirm again the key role of Gln215 in explaining the selectivity of compound **1**. Indeed, this residue provides a remarkable energy contribution to ligand binding equal to  $-3.78(\pm 0.64)$  kcal/mol, a value significantly larger than that provided by the corresponding Gln204 in hMAO-B ( $-1.71(\pm 0.44)$  kcal/mol).

In addition, this analysis allowed us to identify other residues as likely players of h-MAO-A selectivity: the energy contributions due to Ser209, Val210, Cys323 and Leu337 are significantly larger in hMAO-A than those provided by the corresponding residues in hMAO-B (Ser200, Thr201, Thr314 and Leu328, respectively). Notice that two of

**Table 3**  
Free energy contributions (kcal/mol) of hMAO-A and hMAO-B residues to the binding of **1**.

Residue	hMAO-A vs <b>1</b>	hMAO-B vs <b>1</b>
hMAO-A	$\Delta G$	$\Delta G$
Phe112	$-1.09(\pm 0.47)$	$-0.78(\pm 0.37)$
Asn181	$-1.98(\pm 0.96)$	$-1.36(\pm 0.41)$
Phe208	$-2.28(\pm 0.74)$	$-2.85(\pm 0.36)$
Ser209	$-0.80(\pm 0.34)$	$-0.13(\pm 0.05)$
Val210	$-0.73(\pm 0.30)$	$-0.01(\pm 0.04)$
Gln215	$-3.78(\pm 0.64)$	$-1.71(\pm 0.44)$
Cys323	$-0.78(\pm 0.16)$	$-0.16(\pm 0.06)$
Ile325	$-1.12(\pm 0.34)$	$-1.30(\pm 0.26)$
Ile335	$-1.81(\pm 0.34)$	$-1.74(\pm 0.41)$
Leu337	$-0.76(\pm 0.21)$	$-0.22(\pm 0.12)$
Phe352	$-0.90(\pm 0.30)$	$-0.58(\pm 0.21)$
Tyr407	$-1.32(\pm 0.34)$	$-1.37(\pm 0.40)$
FAD	$-1.30(\pm 0.24)$	$-1.84(\pm 0.38)$

these residues differ between the isoforms. In particular, a valine and cysteine in hMAO-A are replaced by two less hydrophobic threonine residues in hMAO-B.

A more difficult to read picture results by the application of MM-GBSA model on hMAO-A vs **2** and hMAO-B vs **2** (Table 4).

As expected, the balance resulting from  $\Delta G_{\text{ele}}$  and  $\Delta G_{\text{pol}}$  is again positive thus indicating that also in these systems the affinity is dominated by hydrophobic interactions. Nevertheless, no substantial difference can be found between the two isoforms considering the obtained  $\Delta G$  values as well as the values resulting from each single contribution to the binding free energy. This is true also considering the  $\Delta G$  contributions to binding provided by each residue of the binding site, whose values do not show any statistically relevant difference between the two isoforms (the interested reader is referred to Table S1 in the Supporting Information). At a first glance, these results would indicate that, based on the obtained MD trajectories and in disagreement with the experimental findings, **2** should show the same affinity toward the two isoforms. It should be noted that the  $\Delta G$  value for monomer II of hMAO-B vs **2** could be strongly overestimated by MM-GBSA. As above reported, **2** establishes a stable water-mediated interaction with FAD in this monomer but this contribution, as well as the entropic contribution due to the presence of the water molecule in the binding site (entropy of the water molecule before and after ligand binding), cannot properly be taken into account by MM-GBSA, since this methodology employs a *continuum* model of the solvent (see experimental section for methodological details). As recently reported (Genheden and Ryde, 2015) in these cases, this approximation can strongly affect the final  $\Delta G$  of binding. In summary, as far as the compound **2** is concerned, the only hypothesis we can realistically draw, based on both classical analysis of MD trajectories and application of MM-GBSA, is that **2** binds with higher affinity hMAO-B by establishing a stable water-mediated interaction with FAD, not allowed in hMAO-A because of its arched conformation within the binding site. It should be emphasized that these results, taken as a whole, allow to better rationalize MAO-isoform selectivity with respect to previous docking simulations providing only a preliminary and incomplete picture that comprises different hypothetical binding modes for each investigated compound (Catto et al., 2006). More specifically, unlike docking-based hypotheses, herein no H-bond interaction is detected between Tyr407 and the coumarin portion of the hMAO-A selective inhibitor. In addition, the described interaction between Gln215 and sulfonate linker takes place orienting the coumarin ring toward the FAD cofactor rather than the entrance cavity (ligand rotation of about 180°) as postulated by docking simulations. Finally, H-bond interactions involving the nitro substituent in position R<sub>2</sub> and both Thr336 and Met324 are not established during MD simulations, again deviating from docking results. Regarding MAO-B selectivity, the role of a water mediated interaction involving the carbonyl oxygen of the coumarin portion and FAD has been hypothesized in one of the putative binding modes provided by previous docking simulations while the possible H-bond interaction between Tyr326 and the oxymethylene bridge was not observed during MD simulations unlike a previous docking-based investigation (Catto et al., 2006).

**Table 4**  
Binding free energy contributions (kcal/mol) in hMAO-A vs **2** and hMAO-B vs **2**.

Terms	hMAO-A vs <b>2</b>		hMAO-B vs <b>2</b>	
	Monomer I	Monomer II	Monomer I	Monomer II
$\Delta G_{\text{vdw}}$	-41.43(±2.77)	-43.41(±2.48)	-43.96(±2.28)	-45.15(±2.19)
$\Delta G_{\text{ele}}$	-10.41(±4.95)	-9.88(±2.79)	-15.91(±2.66)	-7.22(±4.16)
$\Delta G_{\text{pol}}$	23.40(±3.40)	20.08(±2.43)	28.67(±2.01)	22.23(±3.43)
$\Delta G_{\text{nonpol}}$	-5.57(±0.20)	-5.70(±0.15)	-5.74(±0.13)	-5.70(±0.16)
$\Delta H$	-34.00(±3.06)	-38.91(±3.40)	-36.95(±2.38)	-35.85(±2.72)
$\Delta G$	-17.10(±3.06)	-22.48(±3.40)	-18.44(±2.38)	-19.70(±2.72)

## 4. Conclusions

In this study, the combined application of comparative MD simulations and MM-GBSA method provides important clues that can be useful for the design of new and highly isoform-selective MAO inhibitors. We employed as molecular probes two 2H-chromene-2-ones inhibitors whose main structural difference consists in the bridge linking a coumarin scaffold with an aromatic ring. In particular, the emerged picture indicates that a bulky linker having strong H-bond acceptor properties should favor hMAO-A selectivity by allowing a stable H-bond interaction with Gln215, hampered in the binding site of hMAO-B because of its smaller size (Youdim et al., 2006). On the other hand, the presence of a less bulky linker able to preserve a high ligand flexibility seems to favor the hMAO-B selectivity since it allows to establish a highly stable water-mediated interaction with FAD, forbidden in hMAO-A because of a different conformation (arched) of the ligand within its binding site. From a more computational point of view, this work represents the first attempt to account for protein dynamics to rationalize the MAO-isoform selectivity and demonstrates that the static view provided by previous docking simulations should be critically revised.

## Acknowledgments

We acknowledge the CINECA awards nos. HP10C00P06, HP10BWMW76 and HP10CWS1PD under the ISCR initiative for the availability of high-performance computing resources and support. This work was funded under the program FIRB (Futuro in Ricerca 2012, RBFR12SJA8\_003). Leonardo Pisani kindly acknowledges financial support from APQ Research Apulian Region "FutureInResearch" (FKY7YJ5) - Regional program for smart specialization and social and environmental sustainability - Fondo di Sviluppo e Coesione 2007-2013. We wish to thank Angelo Carotti for his wise guide over the years.

## Appendix A. Supplementary data

Supplementary data to this article can be found online at <http://dx.doi.org/10.1016/j.ejps.2017.02.008>.

## References

- Adelman, S.A., Doll, J.D., 1976. Generalized Langevin equation approach for atom/solid-surface scattering: general formulation for classical scattering off harmonic solids. *J. Chem. Phys.* 64:2375–2388. <http://dx.doi.org/10.1063/1.432526>.
- Alberga, D., Mangiatordi, G.F., 2016. Understanding complexity of physiology by combined molecular simulations and experiments: anion channels as a proof of concept. *J. Physiol.* 594:2777–2778. <http://dx.doi.org/10.1113/jp272001>.
- Alberga, D., Nicolotti, O., Lattanzi, G., Nicchia, G.P., Frigeri, A., Pisani, F., Benfenati, V., Mangiatordi, G.F., 2014. A new gating site in human aquaporin-4: insights from molecular dynamics simulations. *Biochim. Biophys. Acta BBA - Biomembr.* 1838: 3052–3060. <http://dx.doi.org/10.1016/j.bbmem.2014.08.015>.
- Allen, W.J., Bevan, D.R., 2011. Steered molecular dynamics simulations reveal important mechanisms in reversible monoamine oxidase B inhibition. *Biochemistry (Mosc)* 50:6441–6454. <http://dx.doi.org/10.1021/bi200446w>.
- Anderson, M.C., Hasan, F., McCrodden, J.M., Tipton, K.F., 1993. Monoamine oxidase inhibitors and the cheese effect. *Neurochem. Res.* 18, 1145–1149.
- Bach, A.W., Lan, N.C., Johnson, D.L., Abell, C.W., Bembenek, M.E., Kwan, S.W., Seeburg, P.H., Shih, J.C., 1988. cDNA cloning of human liver monoamine oxidase A and B: molecular basis of differences in enzymatic properties. *Proc. Natl. Acad. Sci.* 85, 4934–4938.
- Baldessarini, R.J., 1989. Current status of antidepressants: clinical pharmacology and therapy. *J. Clin. Psychiatry* 50, 117–126.
- Bayly, C.I., Cieplak, P., Cornell, W., Kollman, P.A., 1993. A well-behaved electrostatic potential based method using charge restraints for deriving atomic charges: the RESP model. *J. Phys. Chem.* 97:10269–10280. <http://dx.doi.org/10.1021/j100142a004>.
- Binda, C., Li, M., Hubalek, F., Restelli, N., Edmondson, D.E., Mattevi, A., 2003. Insights into the mode of inhibition of human mitochondrial monoamine oxidase B from high-resolution crystal structures. *Proc. Natl. Acad. Sci. U. S. A.* 100:9750–9755. <http://dx.doi.org/10.1073/pnas.1633804100>.
- Binda, C., Wang, J., Pisani, L., Caccia, C., Carotti, A., Salvati, P., Edmondson, D.E., Mattevi, A., 2007. Structures of human monoamine oxidase B complexes with selective noncovalent inhibitors: safinamide and coumarin analogs. *J. Med. Chem.* 50: 5848–5852. <http://dx.doi.org/10.1021/jm070677y>.
- Carotti, A., Carrieri, A., Chimichi, S., Bocalini, M., Cosimelli, B., Gnerre, C., Carotti, A., Carrupt, P.-A., Testa, B., 2002. Natural and synthetic geiparvarins are strong and



- selective MAO-B inhibitors. Synthesis and SAR studies. *Bioorg. Med. Chem. Lett.* 12: 3551–3555. [http://dx.doi.org/10.1016/S0960-894X\(02\)00798-9](http://dx.doi.org/10.1016/S0960-894X(02)00798-9).
- Casacchia, M., Carolei, A., Barba, C., Frontoni, M., Rossi, A., Meco, G., Zylberman, M., 1984. A placebo-controlled study of the antidepressant activity of moclobemide, a new MAO-A Inhibitor. *Pharmacopsychiatry* 17:122–125. <http://dx.doi.org/10.1055/s-2007-1017421>.
- Case, D.A., Betz, R.M., Botello-Smith, W., Cerutti, D.S., Cheatham, T.E., Darden, T.A., Duke, R.E., Giese, T.J., Gohlke, H., Goetz, A.W., Homeyer, N., Izadi, S., Janowski, P., Kaus, J., Kovalenko, A., Lee, T.S., LeGrand, S., Li, P., Lin, C., Luchko, T., Luo, R., Madej, B., Mermelstein, D., Merz, K.M., Monard, G., Nguyen, H., Nguyen, F.T., Omelyan, I., Onufriev, A., Roe, D.R., Roitberg, A., Sagui, C., Simmerling, C.L., Swails, J., Walker, R.C., Wang, J., Wolf, R.M., Wu, X., Xiao, L., York, D.M., Kollman, P.A., 2015. *AMBER 2015*. University of California, San Francisco.
- Catto, M., Nicolotti, O., Leonetti, F., Carotti, A., Favia, A.D., Soto-Otero, R., Méndez-Alvarez, E., Carotti, A., 2006. Structural insights into monoamine oxidase inhibitory potency and selectivity of 7-substituted coumarins from ligand- and target-based approaches. *J. Med. Chem.* 49:4912–4925. <http://dx.doi.org/10.1021/jm0601831>.
- Chimenti, F., Cottiglia, F., Bonsignore, L., Casu, L., Casu, M., Floris, C., Secci, D., Bolasco, A., Chimenti, P., Granese, A., Befani, O., Turini, P., Alcaro, S., Ortuso, F., Trombetta, G., Loizzo, A., Guarino, I., 2006. Quercetin as the active principle of *Hypericum hircinum* exerts a selective inhibitory activity against MAO-A: extraction, biological analysis, and computational study. *J. Nat. Prod.* 69:945–949. <http://dx.doi.org/10.1021/np060015w>.
- Darden, T., York, D., Pedersen, L., 1993. Particle mesh Ewald: an N-log(N) method for Ewald sums in large systems. *J. Chem. Phys.* 98:10089–10092. <http://dx.doi.org/10.1063/1.464397>.
- De Colibus, L., Li, M., Binda, C., Lustig, A., Edmondson, D.E., Mattevi, A., 2005. Three-dimensional structure of human monoamine oxidase A (MAO A): relation to the structures of rat MAO A and human MAO B. *Proc. Natl. Acad. Sci. U. S. A.* 102:12684–12689. <http://dx.doi.org/10.1073/pnas.0505975102>.
- Farina, R., Pisani, L., Catto, M., Nicolotti, O., Gadaleta, D., Denora, N., Soto-Otero, R., Méndez-Alvarez, E., Passos, C.S., Muncipinto, G., Altomare, C.D., Nurisso, A., Carrupt, P.-A., Carotti, A., 2015. Structure-based design and optimization of Multitarget-directed 2H-chromen-2-one derivatives as potent inhibitors of monoamine oxidase B and Cholinesterases. *J. Med. Chem.* 58:5561–5578. <http://dx.doi.org/10.1021/acs.jmedchem.5b00599>.
- Feller, S.E., Zhang, Y., Pastor, R.W., Brooks, B.R., 1995. Constant pressure molecular dynamics simulation: the Langevin piston method. *J. Chem. Phys.* 103:4613–4621. <http://dx.doi.org/10.1063/1.470648>.
- Gaussian 09, Revision E.01, Frisch, M.J., Trucks, G.W., Schlegel, H.B., Scuseria, G.E., Robb, M.A., Cheeseman, J.R., Scalmani, G., Barone, V., Mennucci, B., Petersson, G.A., Nakatsuji, H., Caricato, M., Li, X., Hratchian, H.P., Izmaylov, A.F., Bloino, J., Zheng, G., Sonnenberg, J.L., Hada, M., Ehara, M., Toyota, K., Fukuda, R., Hasegawa, J., Ishida, M., Nakajima, T., Honda, Y., Kitao, O., Nakai, H., Vreven, T., Montgomery, J.A., Peralta, J.E., Ogliaro, F., Bearpark, M., Heyd, J.J., Brothers, E., Kudin, K.N., Staroverov, V.N., Kobayashi, R., Normand, J., Raghavachari, K., Rendell, A., Burant, J.C., Iyengar, S.S., Tomasi, J., Cossi, M., Rega, N., Millam, J.M., Klene, M., Knox, J.E., Cross, J.B., Bakken, V., Adamo, C., Jaramillo, J., Gomperts, R., Stratmann, R.E., Yazyev, O., Austin, A.J., Cammi, R., Pomelli, C., Ochterski, J.W., Martin, R.L., Morokuma, K., Zakrzewski, V.G., Voth, G.A., Salvador, P., Dannenberg, J.J., Dapprich, S., Daniels, A.D., Farkas, O., Foresman, J.B., Ortiz, J.V., Cioslowski, J., Fox, D.J., Gaussian, Inc., 2009. *Wallingford CT*.
- Genheden, S., Ryde, U., 2015. The MM/PBSA and MM/GBSA methods to estimate ligand-binding affinities. *Expert Opin. Drug Discov.* 10:449–461. <http://dx.doi.org/10.1517/17460441.2015.1032936>.
- Gökhan-Keleçi, N., Koyunoglu, S., Yabanoğlu, S., Yelekçi, K., Özgen, Ö., Uçar, G., Erol, K., Kendi, E., Yeşilada, A., 2009. New pyrazoline bearing 4(3H)-quinazolinone inhibitors of monoamine oxidase: synthesis, biological evaluation, and structural determinants of MAO-A and MAO-B selectivity. *Bioorg. Med. Chem.* 17:675–689. <http://dx.doi.org/10.1016/j.bmc.2008.11.068>.
- Hassan, S.Y., Khattab, S.N., Bekhit, A.A., Amer, A., 2006. Synthesis of 3-benzyl-2-substituted quinoxalines as novel monoamine oxidase A inhibitors. *Bioorg. Med. Chem. Lett.* 16:1753–1756. <http://dx.doi.org/10.1016/j.bmcl.2005.11.088>.
- Hou, T., Wang, J., Li, Y., Wang, W., 2011. Assessing the performance of the MM/PBSA and MM/GBSA methods. 1. The accuracy of binding free energy calculations based on molecular dynamics simulations. *J. Chem. Inf. Model.* 51:69–82. <http://dx.doi.org/10.1021/ci100275a>.
- Hu, G., Wang, J., 2014. Ligand selectivity of estrogen receptors by a molecular dynamics study. *Eur. J. Med. Chem.* 74:726–735. <http://dx.doi.org/10.1016/j.ejmech.2013.04.049>.
- Huang, J., MacKerell, A.D., 2013. CHARMM36 all-atom additive protein force field: validation based on comparison to NMR data. *J. Comput. Chem.* 34:2135–2145. <http://dx.doi.org/10.1002/jcc.23354>.
- Hubálek, F., Binda, C., Khalil, A., Li, M., Mattevi, A., Castagnoli, N., Edmondson, D.E., 2005. Demonstration of isoleucine 199 as a structural determinant for the selective inhibition of human monoamine oxidase B by specific reversible inhibitors. *J. Biol. Chem.* 280:15761–15766. <http://dx.doi.org/10.1074/jbc.M500949200>.
- Humphrey, W., Dalke, A., Schulten, K., 1996. VMD: Visual molecular dynamics. *J. Mol. Graph.* 14:33–38. [http://dx.doi.org/10.1016/0263-7855\(96\)00018-5](http://dx.doi.org/10.1016/0263-7855(96)00018-5).
- Jones, G., Willett, P., Glen, R.C., Leach, A.R., Taylor, R., 1997. Development and validation of a genetic algorithm for flexible docking. *J. Mol. Biol.* 267:727–748. <http://dx.doi.org/10.1006/jmbi.1996.0897>.
- Jorgensen, W.L., Chandrasekhar, J., Madura, J.D., Impey, R.W., Klein, M.L., 1983. Comparison of simple potential functions for simulating liquid water. *J. Chem. Phys.* 79:926–935. <http://dx.doi.org/10.1063/1.445869>.
- Kalutkar, A.S., Dalvie, D.K., Castagnoli, N., Taylor, T.J., 2001. Interactions of nitrogen-containing xenobiotics with monoamine oxidase (MAO) isozymes A and B: SAR studies on MAO substrates and inhibitors. *Chem. Res. Toxicol.* 14:1139–1162. <http://dx.doi.org/10.1021/tx010073b>.
- Kaludercic, N., Carpi, A., Nagayama, T., Sivakumaran, V., Zhu, G., Lai, E.W., Bedja, D., De Mario, A., Chen, K., Gabrielson, K.L., Lindsey, M.L., Pacak, K., Takimoto, E., Shih, J.C., Kass, D.A., Di Lisa, F., Paolucci, N., 2013. Monoamine oxidase B prompts mitochondrial and cardiac dysfunction in pressure overloaded hearts. *Antioxid. Redox Signal.* 20:267–280. <http://dx.doi.org/10.1089/ars.2012.4616>.
- Kaludercic, N., Takimoto, E., Nagayama, T., Feng, N., Lai, E.W., Bedja, D., Chen, K., Gabrielson, K.L., Blakely, R.D., Shih, J.C., Pacak, K., Kass, D.A., Lisa, F.D., Paolucci, N., 2010. Monoamine oxidase A-mediated enhanced catabolism of norepinephrine contributes to adverse remodeling and pump failure in hearts with pressure overload. *Circ. Res.* 106:193–202. <http://dx.doi.org/10.1161/CIRCRESAHA.109.198366>.
- Karplus, M., McCammon, J.A., 2002. Molecular dynamics simulations of biomolecules. *Nat. Struct. Biol.* 9:646–652. <http://dx.doi.org/10.1038/nsb0902-646>.
- Karuppasamy, M., Mahapatra, M., Yabanoglu, S., Ucar, G., Sinha, B.N., Basu, A., Mishra, N., Sharon, A., Kulandaivelu, U., Jayaprakash, V., 2010. Development of selective and reversible pyrazoline based MAO-A inhibitors: synthesis, biological evaluation and docking studies. *Bioorg. Med. Chem.* 18:1875–1881. <http://dx.doi.org/10.1016/j.bmc.2010.01.043>.
- Kollman, P.A., Massova, I., Reyes, C., Kuhn, B., Huo, S., Chong, L., Lee, M., Lee, T., Duan, Y., Wang, W., Donini, O., Cieplak, P., Srinivasan, J., Case, D.A., Cheatham, T.E., 2000. Calculating structures and free energies of complex molecules: combining molecular mechanics and continuum models. *Acc. Chem. Res.* 33:889–897. <http://dx.doi.org/10.1021/ar000033j>.
- Kumar, B., Sheetal, Mantha, A.K., Kumar, V., 2016. Recent developments on the structure–activity relationship studies of MAO inhibitors and their role in different neurological disorders. *RSC Adv.* 6:42660–42683. <http://dx.doi.org/10.1039/C6RA00302H>.
- La Regina, G., Silvestri, R., Artico, M., Lavecchia, A., Novellino, E., Befani, O., Turini, P., Agostinelli, E., 2007. New pyrrole inhibitors of monoamine oxidase: synthesis, biological evaluation, and structural determinants of MAO-A and MAO-B selectivity. *J. Med. Chem.* 50:922–931. <http://dx.doi.org/10.1021/jm060882y>.
- Mangiatordi, G.F., Alberga, D., Siragusa, L., Goracci, L., Lattanzi, G., Nicolotti, O., 2015. Challenging AQP4 druggability for NMO-IgG antibody binding using molecular dynamics and molecular interaction fields. *Biochim. Biophys. Acta BBA - Biomembr.* 1848:1462–1471. <http://dx.doi.org/10.1016/j.bbame.2015.03.019>.
- Martínez, L., Nascimento, A.S., Nunes, F.M., Phillips, K., Aparicio, R., Dias, S.M.G., Figueira, A.C.M., Lin, J.H., Nguyen, P., Apriletti, J.W., Neves, F.A.R., Baxter, J.D., Webb, P., Skaf, M.S., Polikarpov, I., 2009. Gaining ligand selectivity in thyroid hormone receptors via entropy. *Proc. Natl. Acad. Sci. U. S. A.* 106:20717–20722. <http://dx.doi.org/10.1073/pnas.0911024106>.
- Matos, M.J., Viña, D., Janeiro, P., Borges, F., Santana, L., Uriarte, E., 2010. New halogenated 3-phenylcoumarins as potent and selective MAO-B inhibitors. *Bioorg. Med. Chem. Lett.* 20:5157–5160. <http://dx.doi.org/10.1016/j.bmcl.2010.07.013>.
- Matos, M.J., Viña, D., Quezada, E., Picciau, C., Delogu, G., Orallo, F., Santana, L., Uriarte, E., 2009. A new series of 3-phenylcoumarins as potent and selective MAO-B inhibitors. *Bioorg. Med. Chem. Lett.* 19:3268–3270. <http://dx.doi.org/10.1016/j.bmcl.2009.04.085>.
- Nicolotti, O., Giangreco, I., Misciocchia, T.F., Carotti, A., 2009. Improving quantitative structure–activity relationships through multiobjective optimization. *J. Chem. Inf. Model.* 49:2290–2302. <http://dx.doi.org/10.1021/ci9002409>.
- Nicolotti, O., Misciocchia, T.F., Carotti, A., Leonetti, F., Carotti, A., 2008. An integrated approach to ligand- and structure-based drug design: development and application to a series of serine protease inhibitors. *J. Chem. Inf. Model.* 48:1211–1226. <http://dx.doi.org/10.1021/ci800015s>.
- Onufriev, A., Bashford, D., Case, D.A., 2000. Modification of the generalized born model suitable for macromolecules. *J. Phys. Chem. B* 104:3712–3720. <http://dx.doi.org/10.1021/jp994072s>.
- Phillips, J.C., Braun, R., Wang, W., Gumbart, J., Tajkhorshid, E., Villa, E., Chipot, C., Skeel, R.D., Kalé, L., Schulten, K., 2005. Scalable molecular dynamics with NAMD. *J. Comput. Chem.* 26:1781–1802. <http://dx.doi.org/10.1002/jcc.20289>.
- Pisani, L., Barletta, M., Soto-Otero, R., Nicolotti, O., Méndez-Alvarez, E., Catto, M., Introcasa, A., Stefanachi, A., Cellamare, S., Altomare, C., Carotti, A., 2013a. Discovery, biological evaluation, and structure–activity and –selectivity relationships of 6'-substituted (E)-2-(Benzofuran-3(2H)-ylidene)-N-methylacetamides, a novel class of potent and selective monoamine oxidase inhibitors. *J. Med. Chem.* 56:2651–2664. <http://dx.doi.org/10.1021/jm4000769>.
- Pisani, L., Catto, M., Leonetti, F., Nicolotti, O., Stefanachi, A., Campagna, F., Carotti, A., 2011. Targeting monoamine oxidases with multipotent ligands: an emerging strategy in the search of new drugs against neurodegenerative diseases. *Curr. Med. Chem.* 18, 4568–4587.
- Pisani, L., Catto, M., Nicolotti, O., Grossi, G., Di Braccio, M., Soto-Otero, R., Méndez-Alvarez, E., Stefanachi, A., Gadaleta, D., Carotti, A., 2013b. Fine molecular tuning at position 4 of 2H-chromen-2-one derivatives in the search of potent and selective monoamine oxidase B inhibitors. *Eur. J. Med. Chem.* 70:723–739. <http://dx.doi.org/10.1016/j.ejmech.2013.09.034>.
- Pisani, L., Farina, R., Catto, M., Iacobazzi, R.M., Nicolotti, O., Cellamare, S., Mangiatordi, G.F., Denora, N., Soto-Otero, R., Siragusa, L., Altomare, C.D., Carotti, A., 2016a. Exploring basic tail modifications of coumarin-based dual acetylcholinesterase–monoamine oxidase B inhibitors: identification of water-soluble, brain-permeant neuroprotective Multitarget agents. *J. Med. Chem.* 59:6791–6806. <http://dx.doi.org/10.1021/acs.jmedchem.6b00562>.
- Pisani, L., Farina, R., Nicolotti, O., Gadaleta, D., Soto-Otero, R., Catto, M., Di Braccio, M., Méndez-Alvarez, E., Carotti, A., 2015. In silico design of novel 2H-chromen-2-one derivatives as potent and selective MAO-B inhibitors. *Eur. J. Med. Chem.* 89:98–105. <http://dx.doi.org/10.1016/j.ejmech.2014.10.029>.
- Pisani, L., Farina, R., Soto-Otero, R., Denora, N., Mangiatordi, G.F., Nicolotti, O., Méndez-Alvarez, E., Altomare, C.D., Catto, M., Carotti, A., 2016b. Searching for multi-targeting Neurotherapeutics against Alzheimer's: discovery of potent AChE-MAO B inhibitors

- through the decoration of the 2H-chromen-2-one structural motif. *Molecules* 21:362. <http://dx.doi.org/10.3390/molecules21030362>.
- Pisani, L., Muncipinto, G., Miscioscia, T.F., Nicolotti, O., Leonetti, F., Catto, M., Caccia, C., Salvati, P., Soto-Otero, R., Mendez-Alvarez, E., Passeleu, C., Carotti, A., 2009. Discovery of a novel class of potent coumarin monoamine oxidase B inhibitors: development and biopharmacological profiling of 7-[(3-chlorobenzyl)oxy]-4-[(methylamino)methyl]-2H-chromen-2-one methanesulfonate (NW-1772) as a highly potent, selective, reversible, and orally active monoamine oxidase B inhibitor. *J. Med. Chem.* 52:6685–6706. <http://dx.doi.org/10.1021/jm9010127>.
- Reis, J., Cagide, F., Chavarria, D., Silva, T., Fernandes, C., Gaspar, A., Uriarte, E., Remião, F., Alcaro, S., Ortuso, F., Borges, F., 2016. Discovery of new chemical entities for old targets: insights on the lead optimization of chromone-based monoamine oxidase B (MAO-B) inhibitors. *J. Med. Chem.* 59:5879–5893. <http://dx.doi.org/10.1021/acs.jmedchem.6b00527>.
- Riederer, P., Danielczyk, W., Grünblatt, E., 2004. Monoamine oxidase-B inhibition in Alzheimer's disease. *Neurotoxicology* 25:271–277. [http://dx.doi.org/10.1016/S0161-813X\(03\)00106-2](http://dx.doi.org/10.1016/S0161-813X(03)00106-2).
- Santana, L., Uriarte, E., González-Díaz, H., Zagotto, G., Soto-Otero, R., Méndez-Álvarez, E., 2006. A QSAR model for in silico screening of MAO-A inhibitors. Prediction, synthesis, and biological assay of novel coumarins. *J. Med. Chem.* 49:1149–1156. <http://dx.doi.org/10.1021/jm0509849>.
- Sastry, G.M., Adzhigirey, M., Day, T., Annabhimoju, R., Sherman, W., 2013. Protein and ligand preparation: parameters, protocols, and influence on virtual screening enrichments. *J. Comput. Aided Mol. Des.* 27:221–234. <http://dx.doi.org/10.1007/s10822-013-9644-8>.
- Saura, J., Nadal, E., van den Berg, B., Vila, M., Bombi, J.A., Mahy, N., 1996. Localization of monoamine oxidases in human peripheral tissues. *Life Sci.* 59, 1341–1349.
- Schrödinger Release 2015-4: Schrödinger Suite 2015-4 Protein Preparation Wizard; Epik version 3.4, Schrödinger, LLC, New York, NY, 2015; Impact version 6.9, Schrödinger, LLC, New York, NY, 2015; Prime version 4.2, Schrödinger, LLC, New York, NY, 2015.
- Shih, J.C., Chen, K., Ridd, M.J., 1999. MONOAMINE OXIDASE: from genes to behavior. *Annu. Rev. Neurosci.* 22:197–217. <http://dx.doi.org/10.1146/annurev.neuro.22.1.197>.
- Son, S.-Y., Ma, J., Kondou, Y., Yoshimura, M., Yamashita, E., Tsukihara, T., 2008. Structure of human monoamine oxidase A at 2.2-Å resolution: the control of opening the entry for substrates/inhibitors. *Proc. Natl. Acad. Sci. U. S. A.* 105:5739–5744. <http://dx.doi.org/10.1073/pnas.0710626105>.
- Van Vliet, I.M., den Boer, J.A., Westenberg, H.G., 1992. Psychopharmacological treatment of social phobia: clinical and biochemical effects of brofaromine, a selective MAO-A inhibitor. *Eur. Neuropsychopharmacol. J. Eur. Coll. Neuropsychopharmacol.* 2, 21–29.
- Vanommeslaeghe, K., Hatcher, E., Acharya, C., Kundu, S., Zhong, S., Shim, J., Darian, E., Guvench, O., Lopes, P., Vorobyov, I., Mackerell, A.D., 2010. CHARMM general force field: a force field for drug-like molecules compatible with the CHARMM all-atom additive biological force fields. *J. Comput. Chem.* 31:671–690. <http://dx.doi.org/10.1002/jcc.21367>.
- Wang, D.-F., Helquist, P., Wiech, N.L., Wiest, O., 2005. Toward selective histone deacetylase inhibitor design: homology modeling, docking studies, and molecular dynamics simulations of human class I histone deacetylases. *J. Med. Chem.* 48: 6936–6947. <http://dx.doi.org/10.1021/jm0505011>.
- Wang, Z.-M., Li, X.-M., Xue, G.-M., Xu, W., Wang, X.-B., Kong, L.-Y., 2015. Synthesis and evaluation of 6-substituted 3-arylcoumarin derivatives as multifunctional acetylcholinesterase/monoamine oxidase B dual inhibitors for the treatment of Alzheimer's disease. *RSC Adv.* 5:104122–104137. <http://dx.doi.org/10.1039/C5RA22296F>.
- Westlund, K.N., Denney, R.M., Kochersperger, L.M., Rose, R.M., Abell, C.W., 1985. Distinct monoamine oxidase A and B populations in primate brain. *Science* 230:181–183. <http://dx.doi.org/10.1126/science.3875898>.
- Weyler, W., Hsu, Y.-P.P., Breakfield, X.O., 1990. Biochemistry and genetics of monoamine oxidase. *Pharmacol. Ther.* 47:391–417. [http://dx.doi.org/10.1016/0163-7258\(90\)90064-9](http://dx.doi.org/10.1016/0163-7258(90)90064-9).
- Youdim, M.B.H., Bakhle, Y.S., 2006. Monoamine oxidase: isoforms and inhibitors in Parkinson's disease and depressive illness. *Br. J. Pharmacol.* 147:S287–S296. <http://dx.doi.org/10.1038/sj.bjp.0706464>.
- Youdim, M.B.H., Edmondson, D., Tipton, K.F., 2006. The therapeutic potential of monoamine oxidase inhibitors. *Nat. Rev. Neurosci.* 7:295–309. <http://dx.doi.org/10.1038/nrn1883>.
- Yu, W., He, X., Vanommeslaeghe, K., Mackerell, A.D., 2012. Extension of the CHARMM general force field to sulfonyl-containing compounds and its utility in biomolecular simulations. *J. Comput. Chem.* 33:2451–2468. <http://dx.doi.org/10.1002/jcc.23067>.
- Zeng, J., Li, W., Zhao, Y., Liu, G., Tang, Y., Jiang, H., 2008. Insights into ligand selectivity in estrogen receptor isoforms: molecular dynamics simulations and binding free energy calculations. *J. Phys. Chem. B* 112:2719–2726. <http://dx.doi.org/10.1021/jp710029r>.